[47]

A. DI GERLANDO , S. FORTUNA , I. VISTOLI

DESIGN ORIENTED ANALYTICAL MODELLING OF LINEAR SYNCHRONOUS ON-BOARD GENERATORS FOR EMS MAGLEV SYSTEMS

ELECTRIMACS 1996

5th International Conference Organized by the Technical Committe N°1
of IMACS
International Association for Mathematics and Computers in Simulation

MODELLING AND SIMULATION OF ELECTRIC MACHINES
CONVERTERS & SYSTEMS

Saint-Nazaire / France
17-18-19 September 1996

5th INTERNATIONAL CONFERENCE

ORGANIZED BY THE TECHNICAL COMMITTEE N°1 OF IMACS

17 - 18 - 19 SEPTEMBER 1996

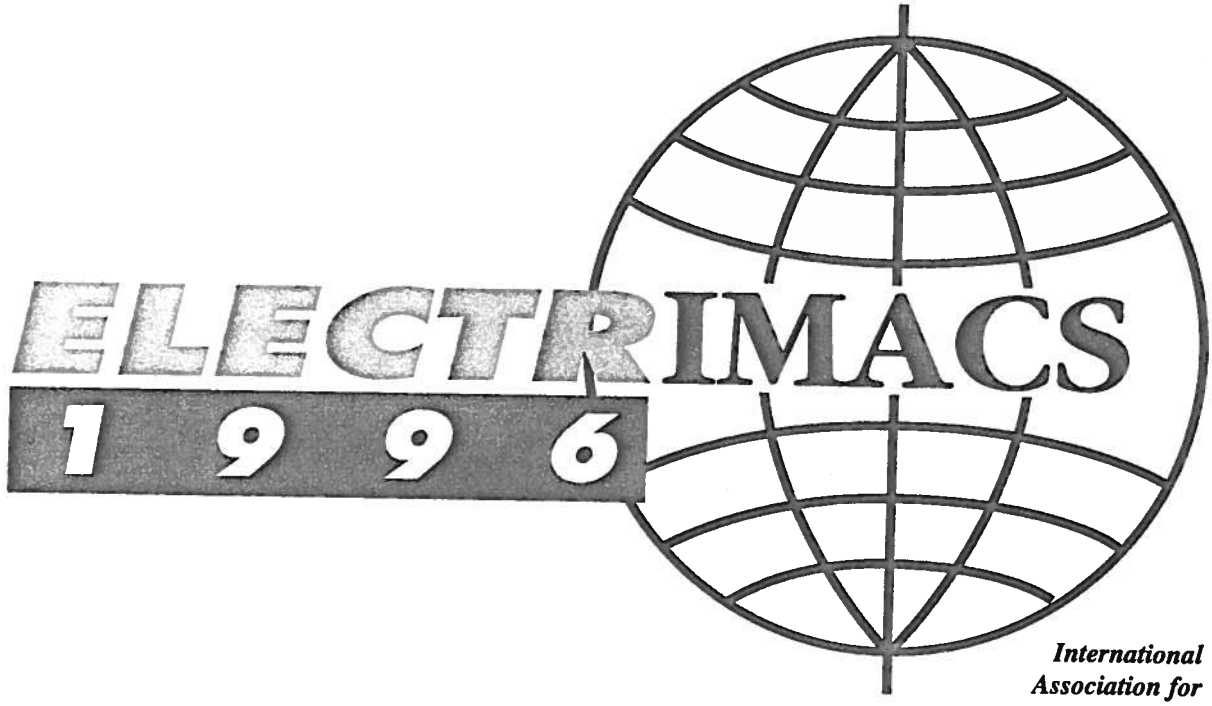

International Association for Mathematics and Computers in Simulation

MODELLING AND SIMULATION OF ELECTRIC MACHINES CONVERTERS & SYSTEMS

Proceedings Vol. 2/3

Saint-Nazaire / France

DESIGN ORIENTED ANALYTICAL MODELLING OF LINEAR SYNCHRONOUS ON-BOARD GENERATORS FOR EMS MAGLEV SYSTEMS

A. DI GERLANDO, S. FORTUNA & I. VISTOLI

DIPARTIMENTO DI ELETTROTECNICA - POLITECNICO DI MILANO
Piazza Leonardo da Vinci 32, 20133 Milano - Italy

Abstract - A method for studying the on-board synchronous generators of EMS Maglev vehicles is described, by means of an approximate analytical model of the air-gap field, verified with the Finite Element Method (FEM): the contributions of induced e.m.f.s due to the m.m.f.s and to the air-gap permeance harmonics are evaluated; a design procedure is developed; the operating characteristics of various types of winding are studied and compared.

1. INTRODUCTION

In the Maglev vehicles driven by a long stator linear synchronous motor (LSM) a suited availability of on board power is required to feed the field windings and the auxiliary services (control, lighting, air-conditioning). The use of on board batteries as stand-alone sources or of brush contacts to transfer the power is awkward; for this reason some devices for the autonomous generation during the running have been developed.
Up to this time only the Linear Synchronous Generator (LSG) has been studied and experimented among the possible solutions: it is realised by disposing suited distributed windings in the part of the LSM pole shoes towards the air-gap.
It is an electrical machine that produces a.c. energy on the basis of two different contributions to the generation of the induced e.m.f.:
- modulation of the air-gap flux, obtained thanks to the reluctance variation generated by the teeth-slot variation between stator guideway and field-levitation pole shoes;
- flux fluctuation due to the harmonic magnetic fields produced by the currents in the stator windings of the LSM.

Subsequently, the energy produced by the LSG is suitably converted by rectifiers and accumulated in storage batteries, however necessary for feeding the on board loads during starts and stops.
The former of the above mentioned contributions is prevailing: in fact, if a vehicle runs inertially along a non-fed guideway section (for example, because of a local fault), actually this e.m.f. term (due to the field m.m.f. only) ensures an emergency supply to the vehicle, though it is reduced.

In the present paper some aspects of the LSG model and design are studied, with reference to the kind of Maglev systems with attractive ElectroMagnetic Suspension (EMS).
The following aspects are considered: the analytical model of the air-gap field (and its comparison with the FEM), the flux evaluation with one or more m.m.f.s, the winding structures and their design and comparison criteria, the waveforms of the LSG no-load operation (when varying the operating conditions of the LSM).

Previous studies on the LSG [1], [2], [3] have already given some preliminary suggestions, considering only the effect of the m.m.f. harmonic fields; even recognising the rough approximation of this approach, these studies gave some hypotheses and conclusions, that define the starting conditions of this analysis:
- the LSM stator currents are considered sinusoidal (thanks to the high frequency of the PWM inverter voltage harmonics and to the high inductance of the fed guideway sections);
- the end effects are neglected;
- the toothed structures have straight teeth with parallel sides;
- the magnetic voltage drops in the ferromagnetic core are neglected (thanks to the great air-gap width and to the low flux density levels, necessary for the levitation control);
- only single-phase windings are analysed: in fact, considering that there are no loads directly fed by the LSG (but only loads at the rectifier output), the number of phases is not a constraint; on the other hand, the space required by a three-phase winding is remarkable, and there are higher constructional difficulties for the high number of crossings between the end-windings.

Work developed with the support of the Italian National Research Council (CNR)

2. PERMEANCES, M.M.F.S AND AIR-GAP FLUXES

The model of the air-gap field is an approximate analytical one, and the evaluation of the corresponding permeances is based on a schematisation of the field lines, similar to the real map: fig.1a shows the real aspect of the air-gap field generated by the LSM field m.m.f. only (obtained by means of the FEM), and fig.1b shows the graphical approximated representation of this field, for a generic position between the stator and one pole shoe with 7 teeth placed on the vehicle. This schematisation is based on the replacement of the field lines with straight line segments (in the air-gap zone) and circumference arcs (in the zone of the teeth sides) and it is justified by the following remarks:
- considering that we are interested not in the local quantities, but only in the integral quantities (permeances, fluxes), the effect of local errors, with variable sign, is inclined to be compensated;
- the permeance evaluation can be improved, by means of a correction coefficient (ν) calibrated by means of the Carter's factor.

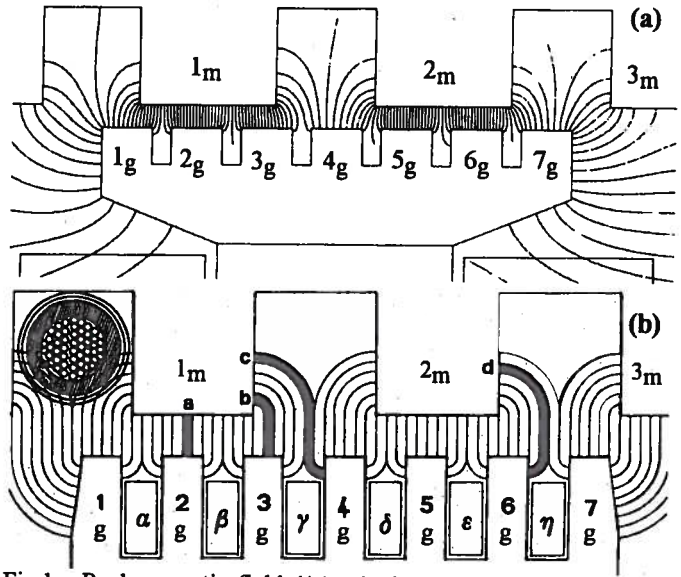

Fig.1 - Real magnetic field ((a), obtained by the FEM) and approximated field ((b), schematised by straight lines -in the air-gap- and circumference arcs - reaching the slot sides).

The proportions of fig.1a refer, as the other parts of the analysis, to a Maglev system with the data of Table I and with a LSM that operates according to the phasor diagram of fig.2.

Tab. I - Main data of the considered EMS Maglev system .

maximum speed v [km/h]; full load weight [t]	500; 120
train length [m]; LSM pole pitch τ_m [m]	54 ; 0.3
feeding inverter maximum frequency f_m [Hz]	231.5
pole shoe length b; motor width, each side ℓ [m]	0.2; 0.2
N° slots/(pole·phase); N° of field poles per side p	1; 150
width b_{sm} and height h_{sm} of the LSM slot [mm]	42; 43
LSM tooth width b_{tm} ; air-gap width δ [mm]	58; 10
LSM current I_s [kA] and line-to-line voltage V_s [kV]	1; 2.5
air-gap flux density under the pole shoe B_f [T]	0.5
phase displacement between I_s and E_s rated angle γ_n [°]	15
reactances X_d e X_q [Ω] of each guideway fed section	1.61; 1.4
slot b_{sg} and tooth b_{tg} widths of the "7 teeth" LSG [mm]	8; 21.71
slot b_{sg} and tooth b_{tg} widths of the "3 teeth" LSG [mm]	16; 56

From the images of fig.1 we can conclude that it is possible to classify the flux tubes according to four fundamental types:
- tube "a", with *I* shape, that develops among the teeth heads;
- tube "b", with *L* shape, that develops between the tooth head of one structure and the tooth side of the other one;
- tubes "c" and "d", with shape *S* and *C* respectively.

The advantage of this model is the simplicity of the analytical expressions of the permeance contributions: for example, in the following the four described flux tubes are shown (fig.3), and the corresponding expressions of the specific permeances are given (H/m), as a function of the dimensions of fig.3 and of the cited coefficient ν, applied as a factor to the geometrical length of the circular arcs of the field lines (equal to 1/4 of a circumference).

$$\lambda_a = \mu_o \cdot \int_0^{b_a} \frac{dx}{\delta} = \mu_o \cdot \frac{b_a}{\delta} \qquad (1)$$

$$\lambda_b = \mu_o \cdot \int_0^{b_b} \frac{dy}{\delta + \nu\cdot(\pi/2)\cdot y} = \mu_o \cdot \frac{2}{\nu\cdot\pi} \cdot \ell n\left(1 + \nu\cdot\frac{\pi}{2}\cdot\frac{b_b}{\delta}\right) \qquad (2)$$

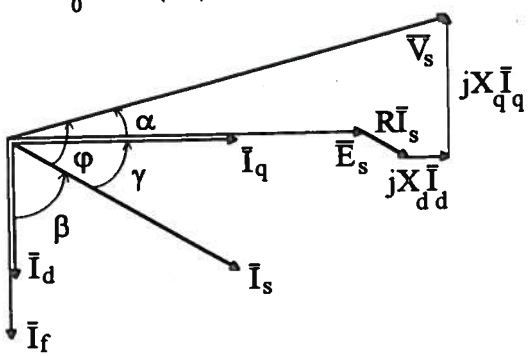

Fig.2 - LSM operation phasor diagram.

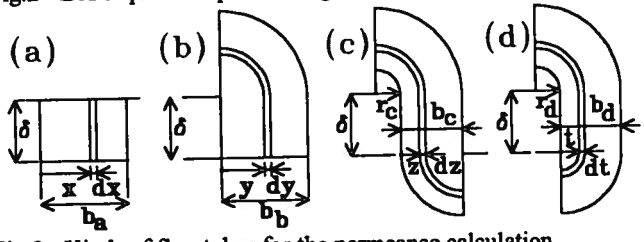

Fig.3 - Kinds of flux tubes for the permeance calculation.

$$\lambda_c = \int_0^{b_c} \frac{\mu_o \cdot dz}{\delta + \nu\cdot\frac{\pi}{2}\cdot(r_c + z) + \nu\cdot\frac{\pi}{2}\cdot(b_c - z)} = \frac{\mu_o \cdot b_c}{\delta + \nu\cdot\frac{\pi}{2}\cdot(r_c + b_c)} \qquad (3)$$

$$\lambda_d = \int_0^{b_d} \frac{\mu_o \cdot dt}{\delta + \nu\cdot\frac{\pi}{2}(r_d + t) + \nu\cdot\frac{\pi}{2}\cdot t} = \frac{\mu_o}{\nu\cdot\pi} \cdot \ell n\left(1 + \frac{\pi\cdot b_d}{\delta + \nu\cdot\frac{\pi}{2}\cdot r_d}\right) \qquad (4)$$

In order to allow the use of these analytical expressions it is necessary to evaluate the value of ν; to this aim the following is made:
- let us consider a toothed structure with straight teeth (with slot pitch τ_s, slot width b_s and tooth width b_t) faced to a smooth structure by means of an air-gap having width δ;
- by applying the previous model, the expression of the specific air-gap permeance λ_t of one tooth (extended within a tooth pitch, between the axes of the adjacent slots) is given by:

$$\lambda_t = \frac{\mu_o \cdot b_t}{\delta} + 2\cdot\mu_o \cdot \int_0^{b_s/2} \frac{dx}{\delta + \nu\cdot(\pi/2)\cdot x} \; ; \qquad (5)$$

- the same permeance can be evaluated in the following manner:

$$\lambda_t = \mu_o \cdot \tau_s / (K_c \cdot \delta) \; , \qquad (6)$$

where K_c , Carter's factor, can be expressed as follows [4]:

$$K_c = \frac{1}{1 - b_s/\tau_s + 2\cdot(\delta/\tau_s)\cdot\ell n\left(1 + b_s/(2\cdot\delta)\right)} \; ; \qquad (7)$$

- by equating the result of (5) with (6), for ν the following occur:

$$\nu = 2/\pi \; . \qquad (8)$$

This correction coefficient, deduced for a particular situation, is assumed not varying for all the types of flux tubes.
In conclusion, from (8) follows that, to the aim of evaluating the air-gap permeances (by (1)-(4)), the sides of straight teeth must be considered inclined by 1 radian with reference to the horizontal.

Of course, when considering the variation of the relative position between the toothed structures, the limits of the integrals (1)-(4) change: thus, it is necessary to consider all the possible configurations, when varying dimensions and position.

For a pole shoe with 7 teeth of a Maglev system with the data of Table I, by (1)-(4) the specific permeance $\lambda_{1g.2m}$ has been evaluated, between the LSG tooth 1_g and the LSM tooth 2_m only, as a function of the position x of the pole shoe (fig.4).

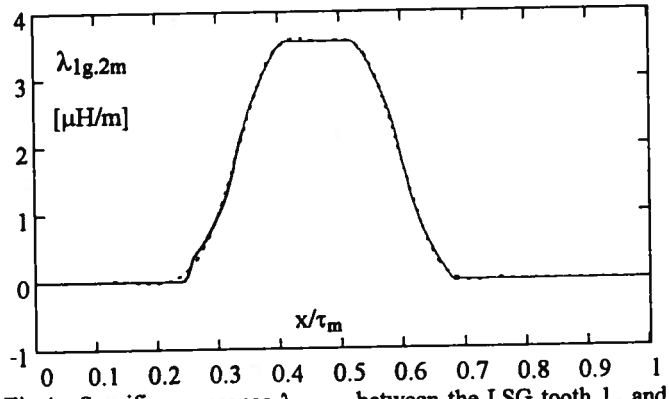

Fig.4 - Specific permeance $\lambda_{1g.2m}$ between the LSG tooth 1_g and the LSM tooth 2_m only (fig.2a), when varying the position x of the pole shoe (measured between the left edge of the tooth 1_g and the axis of the slot preceding the tooth 1_m): —— = curve evaluated by (1)-(4); - - - - - = curve obtained with the first 8 harmonics of the Fourier series evaluated by adopting the pitch τ_m of the LSM as a spatial period and putting $\lambda_{1g.2m}(x) = 0$ for $x < 0$ and for $x > \tau_m$.

The position x (expressed in p.u., referred to the LSM pole pitch τ_m) is zero when the left edge of the tooth 1_g is aligned with the axis of the slot at the left of the tooth 1_m (in fig.1a: x = 10 mm).
We note that the permeance between the teeth 1_g and 2_m is not zero only when they are totally or partially faced.
In fig.4, the continuous curve represents the permeance directly obtained by applying (1)-(4), while the dotted line has been obtained by the previous one, by evaluating the coefficients Λ_j of the Fourier series up to a suited order harmonic (in the present case: j_{max} = 8), by assuming τ_m as a spatial period and making $\lambda_{1g.2m}(x)$ zero for x < 0 and for x > τ_m. In the following, this second formulation of $\lambda_{1g.2m}(x)$ is used: in fact, the permeance obtained by (1)-(4) comes from integrals whose limits are defined, when varying x, by means of suited combinations of Heaviside step functions $H(x-\xi)$ (H = 0 for $x<\xi$; H = 1 for $x\geq\xi$): for this reason, the original $\lambda_{1g.2m}(x)$ is affected by some irregularities that, even if not significant for the same $\lambda_{1g.2m}(x)$, nevertheless cause some discontinuites in its x-derivatives; the use of the truncated Fourier series implies a smoothing effect, respecting the low frequency spatial behaviour.
In conclusion, for $\lambda_{1g.2m}(x)$ the following expression is obtained:

$$\lambda_{1g.2m}(x)=\left(\Lambda_o+\sum_{j=1}^{j_{max}}\Lambda_{c_j}\cdot\cos\left(j\cdot 2\cdot\pi\cdot\frac{x}{\tau_m}\right)+\right.$$
$$\left.+\sum_{j=1}^{j_{max}}\Lambda_{s_j}\cdot\sin\left(j\cdot 2\cdot\pi\cdot\frac{x}{\tau_m}\right)\right)\cdot\left[H(x)-H(x-\tau_m)\right] \quad , \quad (9)$$

where Λ_o is the average value of $\lambda_{1g.2m}$ in the τ_m interval.

1_g is a tooth at the pole shoe side: fig.1a shows that its field lines are similar to those of the intermediate teeth ones, and actually the additional lateral lines are leakage lines towards the adjacent poles: thus, these interpolar fluxes do not contribute to the LSG induced e.m.f. because they are position-independent; thus, all the teeth of a LSG pole shoe can be modelled in the same way.

The permeances among different pairs of teeth have the same waveform as $\lambda_{1g.2m}(x)$, except for a spatial displacement; thus, it is possible to modify (9) as follows: called k_g and k_m the generic LSG and LSM tooth respectively (both numbered from left to right, starting from the teeth 1_g and 1_m of fig.1), we have:
- the permeance among the teeth k_g and 2_m equals:

$$\lambda_{kg.2m}(x)=\lambda_{1g.2m}\left(x+\tau_{sg}\cdot(k_g-1)\right) , \quad (10)$$

where τ_{sg} is the LSG slot pitch ($\tau_{sg} = b_{tg} + b_{sg}$);
- the permeance between the teeth k_g and k_m equals:

$$\lambda_{kg.km}(x)=\lambda_{kg.2m}\left(x-\tau_{sm}\cdot(k_m-2)\right) , \quad (11)$$

where τ_{sm} is the LSM slot pitch ($\tau_{sm} = b_{tm} + b_{sm} = \tau_m/3$);
- thus, putting together (10) and (11), one obtains:

$$\lambda_{kg.km}(x)=\lambda_{1g.2m}\left(x+\tau_{sg}\cdot(k_g-1)-\tau_{sm}\cdot(k_m-2)\right) . \quad (12)$$

When in the air-gap only the field m.m.f. acts (as in fig.1a,b), in general each LSG tooth delivers (or receives) flux from more than one LSM tooth: all these flux tubes are submitted to the same magnetic voltage drop at the air-gap (equal to the field m.m.f., if we neglect the iron core magnetic voltage drops); thus, the global permeance at the air-gap of the tooth k_g towards the toothed LSM stator structure (indicated with $\lambda_{kg.m}$) equals:

$$\lambda_{kg.m}(x)=\sum_{k_m}\lambda_{kg.km}(x) . \quad (13)$$

In (13), the sum is theoretically extended to all the teeth of the stator, but in practice only the k_m teeth of the LSM that actually interact with the tooth k_g must be considered. In one LSM operating period T the vehicle covers a distance of 2 pole pitches ($2\cdot\tau_m$), i.e. a distance equal 6 LSM slot pitches ($6\cdot\tau_{sm}$), finally reaching again the same initial configuration: for this reason it is necessary to consider at least 9 stator teeth in order to develop the analysis during the motion of just one pole shoe (in the present case we have considered 12 stator teeth).

Of course, for (13) a translation property similar to that of each component term can be used, expressed by (12); therefore, for the LSG teeth k'_g and k''_g we can write:

$$\lambda_{k''_g.m}(x)=\lambda_{k'_g.m}\left(x+\tau_{sg}\cdot(k''_g-k'_g)\right) . \quad (14)$$

Fig.5 shows $\lambda_{kg.m}(x)$ for the tooth 4_g of the LSG with 7 teeth: the analytical model (continuous line) is compared with the FEM (values represented with ▫). The following can be observed:
- the FEM calculations refer to the magnetic structure of fig.1a, where we have imposed permeability $\mu_{fe}\rightarrow\infty$ into the ferromagnetic branches: the value of $\lambda_{4g.m}$ has been obtained as ratio among the difference of the magnetic vector potentials in the corners at the basis of the tooth 4_g and the pole shoe m.m.f. M_f;
- a smoothing technique similar to that used for $\lambda_{kg.km}(x)$ has been used for the computations by the analytical model, with the following difference: $\lambda_{kg.m}(x)$ has been evaluated inserting in (13) the original expressions (1)-(4) of the $\lambda_{kg.km}(x)$; in fact, considering that $\lambda_{kg.m}(x)$ is intrinsically a periodic function with spatial period $\tau_{sm} = \tau_m/3$ (see fig.5), it is more convenient to obtain directly from it the Fourier series, instead of summing expressions like (9); thus, $\lambda_{kg.m}(x)$ is given by:

$$\lambda_{kg.m}(x)=\Lambda_{\delta_o}+\sum_{j=1}^{j_{max}}\Lambda_{\delta c_j}\cdot\cos(j\cdot 2\cdot\pi\cdot x/\tau_{sm})+$$
$$+\sum_{j=1}^{j_{max}}\Lambda_{\delta s_j}\cdot\sin(j\cdot 2\cdot\pi\cdot x/\tau_{sm}) \quad ; \quad (15)$$

- while the permeance $\lambda_{kg.km}(x)$ is zero outside the spatial interval of interfacing between the teeth k_g and k_m, the permeance $\lambda_{kg.m}(x)$ presents maxima and minima and it never equals zero, because always a tooth exists that faces it, even if the stator teeth faced to the tooth k_g change;
- there are two reasons for the choice of the tooth 4_g : the behaviour of its specific permeance can be more easily realised (for x = 0, 4_g is aligned with the axis of the slot between 1_m e 2_m, and thus the permeance $\lambda_{4g.m}(0)$ is minimum); moreover, the tooth 4_g is not affected (differently from 1_g and 7_g) by the interpolar leakage fluxes, that would alter the comparison.

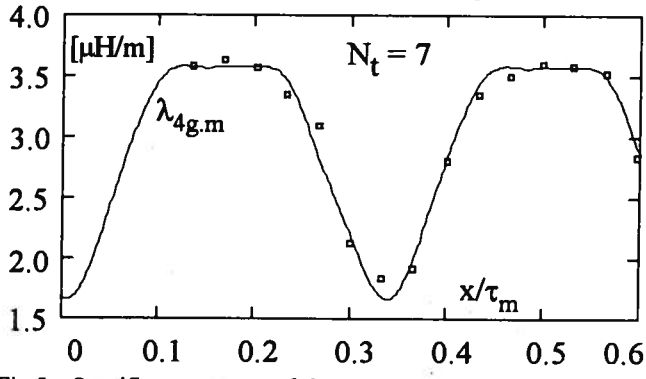

Fig.5 - Specific permeance of the tooth 4_g of the LSG for a pole shoe with 7 teeth, towards the stator LSM global structure, as a function of the position x of the pole shoe:
——— = curve evaluated by applying the analytical model;
▫▫▫ = values evaluated by the Finite Element Method.

In conclusion, fig.5 suggests that the differences between numerical and analytical models are limited and with alternate signs, so that the attribution of the errors is uncertain.

For the moment we suppose that in the air-gap only the field m.m.f. M_f is present: this m.m.f. is time-constant (neglecting the regulation, not considered in this analysis); moreover, M_f acts with the same value on all the air-gap permeances; it follows that, in the pole shoe position x, the tooth k_g of the LSG is interested by the following flux, due to the field m.m.f.:

$$\varphi_{kgf}(x) = M_f \cdot \lambda_{kg.m}(x) \cdot \ell \ , \qquad (16)$$

that varies during the time for effect of the air-gap permeance modulation. The knowledge of the fluxes $\varphi_{kgf}(x(t))$ of the LSG allows to evaluate the flux linkage of the winding $\psi_{gf}(x(t))$:

$$\psi_{gf}(x) = \sum_{kg=1}^{N_t} L_{kg} \cdot \varphi_{kgf}(x) , \qquad (17)$$

where N_t is the number of teeth of the pole shoe and L_{kg} is the linkage coefficient of the tooth k_g (L_{kg} is an integer, equal to the number of linkages of the tooth k_g with the winding, with the suited sign, depending on the sense of winding).

Known the flux linkage, the LSG induced e.m.f. e_g equals:

$$e_{gf}(x) = \frac{d\psi_{gf}}{dt} = \frac{d\psi_{gf}(x)}{dx} \cdot v = v \cdot M_f \cdot \sum_{kg=1}^{N_t} L_{kg} \cdot \frac{d\lambda_{kg.m}}{dx} \cdot \ell \ . \qquad (18)$$

If, as supposed, the LSG winding feeds a single-phase Graetz rectifying bridge, then the rectified no-load voltage equals:

$$v_{do}(x(t)) = \left| e_{gf}(x(t)) \right| \ . \qquad (19)$$

Now we consider existing in the air-gap only the m.m.f. produced by the LSM stator currents (that for the above mentioned hypotheses consist of a tern of balanced sinusoidal currents). This situation, useful for the separated analysis of the phenomena, is not very realistic but anyway not impossible (it may occur if the group of pole shoes of one field unit of the Maglev vehicle is not excited -for example because of a fault-, but the corresponding LSG windings are submitted to the effect of the LSM currents).

At a certain speed, the operating conditions of the LSM imply that, in case of variation of the angle γ, allowed by the control system, the RMS value of the current I_s varies in such a way to maintain constant the component I_q, from which the thrust depends, i.e. the following condition must be satisfied (see fig.2):

$$I_q = I_s \cdot \cos(\gamma) = I_n \cdot \cos(\gamma_n) \ ; \qquad (20)$$

this means that the LSM m.m.f. modifies its amplitude and spatial displacement when changing the motor operating conditions.

In order to evaluate the fluxes flowing in the LSG teeth and generated by the LSM m.m.f., the classical hypothesis to suppose the LSM total slot current concentrated along the axis of the slot itself is adopted; in fact:

- if the height of the stator slots is not too small, we can assume that practically all the field lines reach the tooth sides, not reaching the slot bottom;
- if the active conductors are disposed as in fig.1, it can be assumed that no field line crosses these conductors in a significant amount, i.e. all the field lines are totally linking lines.

Thus, the m.m.f. due to the LSM currents can be represented by means of a spatial function with the following properties:

- in a certain instant, the m.m.f. acting between the slot axes including a stator tooth is constant, and it differs from the m.m.f. of the adjacent teeth by the total currents of the interposed slots;
- the LSM m.m.f. distribution at the air-gap is given by a sequence of steps: the amplitude and the sign of the m.m.f. step of each LSM tooth varies continuously during the time.

Also for the model of this m.m.f. field, running at the air-gap, it is possible to use the Haeviside step functions $H(\bullet)$: called a, b ,c the LSM phases, the m.m.f. of the LSM $m_m(\xi,t)$ (seen by an observer positioned in ξ at the time instant t) is given by:

$$m_m(\xi,t) = m_a(\xi,t) + m_b(\xi,t) + m_c(\xi,t) \ , \quad \text{where} \qquad (21)$$

$$m_a = \hat{I}_s(\gamma) \cdot \cos(\omega \cdot t - \gamma) \cdot \left[H\left(\sin\left(\frac{\pi \cdot \xi}{\tau_m} \right) \right) - \frac{1}{2} \right]$$

$$m_b = \hat{I}_s(\gamma) \cdot \cos\left(\omega \cdot t - \gamma - \frac{2 \cdot \pi}{3} \right) \cdot \left[H\left(\sin\left(\frac{\pi \cdot \xi}{\tau_m} - \frac{2 \cdot \pi}{3} \right) \right) - \frac{1}{2} \right] \ . \qquad (22)$$

$$m_c = \hat{I}_s(\gamma) \cdot \cos\left(\omega \cdot t - \gamma + \frac{2 \cdot \pi}{3} \right) \cdot \left[H\left(\sin\left(\frac{\pi \cdot \xi}{\tau_m} + \frac{2 \cdot \pi}{3} \right) \right) - \frac{1}{2} \right]$$

Eq.(22) depends explicitly on the phase γ, according to (20). Actually, as already observed, in a certain instant the m.m.f. $m_{mkm}(t)$ acting on the tooth k_m is constant for an extension equal to τ_{sm} ; thus, by applying (21) we can write:

$$m_{mkm}(t) = m_m\left((k_m - 1) \cdot \tau_{sm}, t \right) \ . \qquad (23)$$

For example, fig.6 shows the m.m.f. acting on the stator teeth, for $x = t = 0$, with $\gamma = \gamma_n$: in the initial instant the magnetic axis of the LSM m.m.f. is near the tooth 3_m (see fig.s 1 and 2), i.e. in the correct position in order to apply the alignment influence on the field pole, whose axis, that coincides with the tooth 4_g , has a delay of β spatial radians, in the motion sense.

When only the m.m.f. $m_{mkm}(t)$ is acting, the flux in the tooth k_g of the LSG is given by the contributions of all the flux tubes coming from the LSM teeth faced to it, proportionally to the permeance of every tube and to the m.m.f. acting upon each of them:

$$\varphi_{kg_m}(x(t),t) = \ell \cdot \sum_{k_m} \lambda_{kg.km}(x(t)) \cdot m_{mkm}(t) \ . \qquad (24)$$

From (24) the calculations are similar to those seen for the operation with the field m.m.f. M_f only; the flux linkage is:

$$\psi_{gm}(x(t),t) = \sum_{k_g=1}^{N_t} L_{kg} \cdot \varphi_{kg_m}(x(t),t) \ , \qquad (25)$$

and thus the induced e.m.f. in the LSG is given by:

$$e_{gm}(t) = v \cdot \sum_{k_g=1}^{N_t} L_{kg} \cdot \frac{d\lambda_{kg.m}}{dx} \cdot \ell \cdot m_{mkm}(t) + \sum_{k_g=1}^{N_t} L_{kg} \cdot \frac{d(m_{mkm}(t))}{dt} \cdot \ell \lambda_{kg.km}(x(t)) \ ; \qquad (26)$$

from (26) the double nature of the e.m.f. $e_{gm}(t)$ can be recognised:

- the first term, of motional kind (similar to that due to M_f), is generated by the main field of the LSM, whose flux, synchronous with the vehicle, is modulated by the tooth-slot variations;
- the second term, of transformatoric kind, can be also explained with the related motion of the LSM harmonic m.m.f. fields running at the air-gap as regards the vehicle.

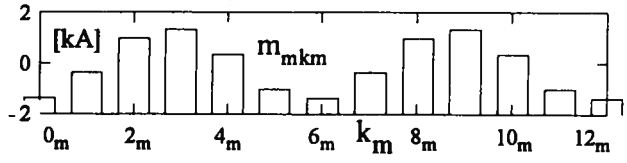

Fig.6 - Distribution of the step m.m.f. m_{mkm} produced under each LSM tooth k_m from the currents of the LSM itself, for $\gamma = \gamma_n$, in the instant $t = 0$ (in which $x = 0$).

The possibility to apply the superposition theorem comes from the hypothesis of magnetically linear circuit:

$$e_{gt}(t) = \frac{d\psi_g}{dt} = \frac{d\psi_{gf}}{dt} + \frac{d\psi_{gm}}{dt}; \qquad (27)$$

$$v_{dot}(t) = |e_{gt}(t)| = |e_{gf}(t) + e_{gm}(t)| . \qquad (28)$$

Finally, it must observed that, thanks to the synchronous operation (v = constant), in the previous equations the time dependence can be always expressed as a function of the vehicle position:

$$t = x/v . \qquad (29)$$

The following figures show the teeth fluxes waveforms for a pole shoe with 7 teeth (data of Table I); it can be observed that:
- the tooth fluxes produced by M_f only (fig.7) reproduce exactly the permeance waveform of fig.5: they have the same shape for different teeth, with a time shift corresponding to the teeth spatial displacement, and their frequency equals 6 times f_m;
- the fluxes produced in the same teeth by the m_{mkm} only (fig.8) show the same phases of the previous ones, but different waveforms (because subjected to different m.m.f.s, see fig.6) with a smaller flux variation compared to that generated by M_f;
- the flux waveforms produced by both the 2 m.m.f.s (fig.9) appear similar to those ones of fig.7: the LSM m.m.f. produces a waveform distortion and a change of the average values, but it modifies in a more limited amount the peak-to-peak variation $\Delta\varphi_{p\text{-}p}$ of different teeth;
- fig.10 shows the effect of doubling the angle γ, according to (20): it can be noted a slight increase of the variation $\Delta\varphi_{p\text{-}p}$, but, above all, an increase of the average value of the flux itself: this is due to the reinforcing of the m.m.f. at the air gap, exerted by the I_d current component, accordingly to fig.2.

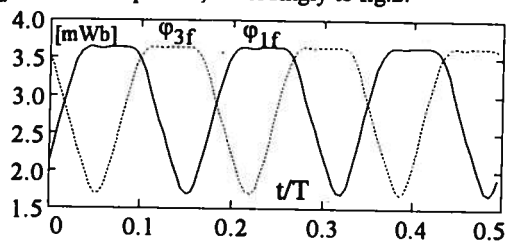

Fig.7 - Flux of the teeth g_1 and g_3, due to the field m.m.f. M_f only.

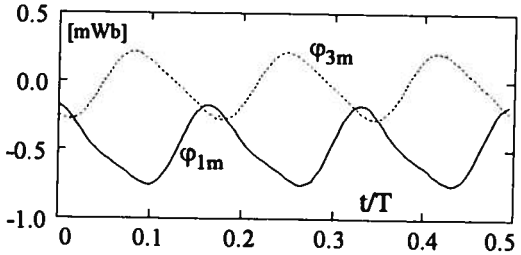

Fig.8 - Flux of the teeth g_1 and g_3, due to the LSM m.m.f. only.

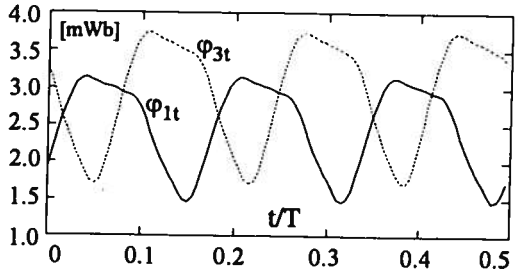

Fig.9 - Flux of the teeth g_1 and g_3, due to the field m.m.f. M_f and to the LSM m.m.f., acting simultaneously.

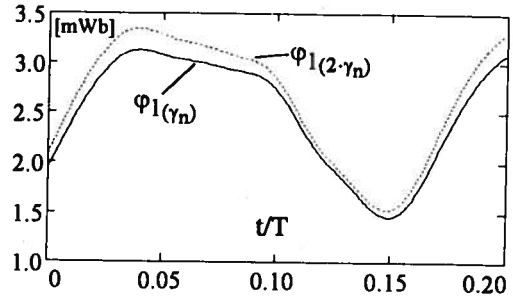

Fig.10 - Flux in the tooth g_1, due to the field m.m.f. and to the LSM m.m.f., for $\gamma = \gamma_n$ and $\gamma = 2\cdot\gamma_n$.

3. LSG DESIGN CRITERIA

By means of the above described model, the LSG windings, whose schemes are shown in fig.11, have been examined: they are windings that, for comparison needs, have the common characteristic of possessing the same number of active sides disposed in the pole shoe. As known, each active side can consist of several conductors (i.e. each coil can have more turns): thus, according to the classical representation modes of the windings, in the schemes of fig.11 each coil is represented as like as it would contain just one turn. In the present case we suppose that each active side contains just one conductor; thus, the total number of conductors of each winding is: U = 8.

It can be realised that the only structures that allow windings with U = 8 are those with N_t = 7 teeth (with u = 1 conductor/slot) and those with N_t = 3 teeth (with u = 2 conductors/slot); we consider useful slot also the space available at the sides of the pole shoes.

The windings of fig.11 can be classified as follows:
- windings for pole shoes with 7 teeth (A,B,C,D) or 3 teeth (E,F);
- single part (A,B,E) or subdivided (C,D,F) windings.

As an example, the waveforms of the winding B are shown:
- fig.12 shows that the flux linkage has a non-zero average value and that this value depends on the LSM m.m.f.;
- the variation $\Delta\psi_{pp}$ depends weakly on the additional presence of the LSM m.m.f, as confirmed by the small variation of the induced e.m.f. of fig.13;
- fig.14 shows the rectified no-load voltage and its average value, when only the field m.m.f. M_f is present;
- finally, fig.15 shows the increase of the rectified voltage when the angle γ of the LSM m.m.f. grows: nevertheless, the increase of V_{do} is quite limited compared with the value in the operation when only the m.m.f. M_f acts.

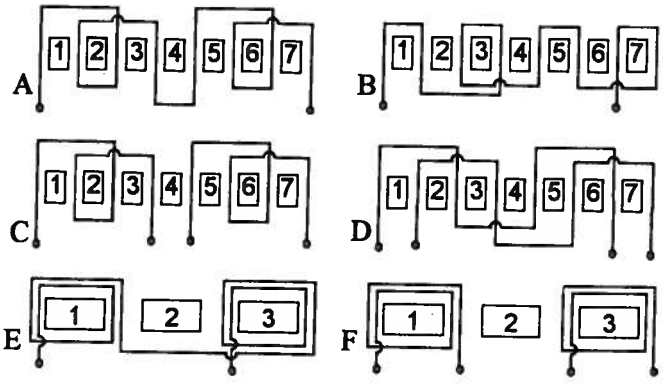

Fig.11 - Schemes of single-phase windings for LSG:
A, B, C; D = windings for pole shoes with 7 teeth;
E, F = windings for pole shoes with 3 teeth.

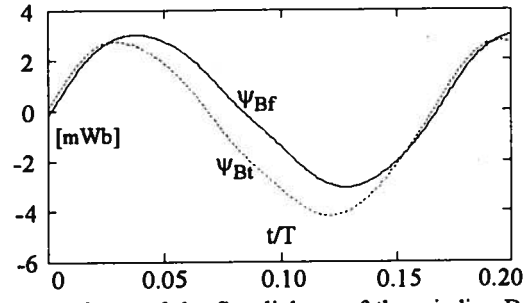

Fig.12 - Waveforms of the flux linkage of the winding B, due to the M_f only (ψ_{Bf}) and total (due to M_f and m_{mkm}: ψ_{Bt}); $\gamma = \gamma_n$.

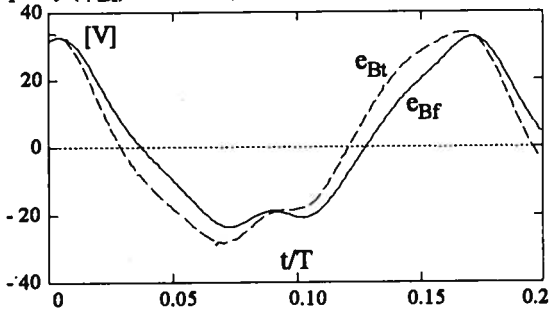

Fig.13 - E.m.f. induced in the winding B, produced by the M_f only (e_{Bf}) and by the sum of M_f and of m_{mkm} (e_{Bt}), with $\gamma = \gamma_n$.

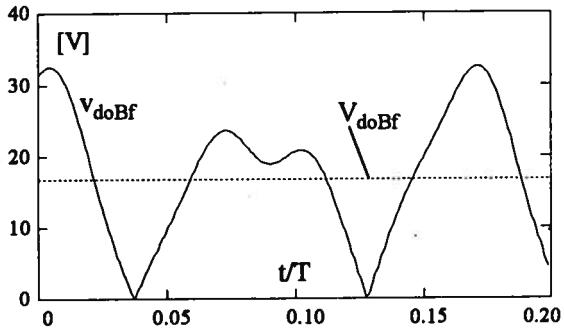

Fig.14 - No-load rectified voltage obtained by the winding B excited by M_f (v_{doBf}) and corresponding average value (V_{doBf}).

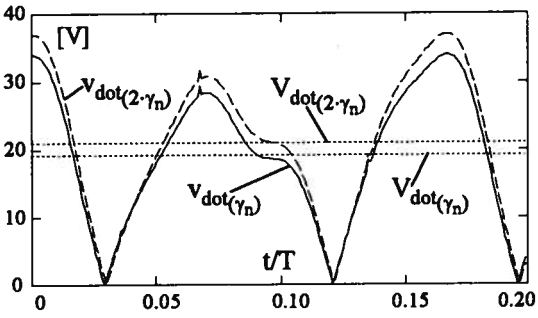

Fig.15 - Waveforms and average values of the no-load rectified voltage of the winding B, with M_f and m_{mkm} ($\gamma = \gamma_n$ and $\gamma = 2\cdot\gamma_n$).

These results suggest the following remarks:
- the prevailing part of the e.m.f. is produced by the m.m.f. M_f, that, to the aim of the design, can be considered as acting alone;
- fig.s 12 and 13 show that the prevailing harmonic is the main one (with frequency 6 times the LSM one, f_m): thus, also in the tooth permeance $\lambda_{kg.m}(x)$ the main harmonic prevails (see (15) and fig.5), with spatial period τ_{sm} and amplitude Λ_I given by:

$$\Lambda_I = \sqrt{(\Lambda_{\delta c1})^2 + (\Lambda_{\delta s1})^2} \quad ; \qquad (30)$$

- considering that, for (29), all the previous equations link quantities with practically sinusoidal spatial and time waveforms, they can be transformed in the corresponding relationships between phasors: (16), expressing the tooth flux phasor, and (17), that performs the teeth fluxes phasor sum, are particularly important.

Called Φ and Ψ the first harmonic peak amplitudes of the tooth flux and of the winding flux linkage respectively, and called $\Delta\Psi_{pp} = 2\cdot\Psi$, the output voltage V_{do} of a single-phase bridge equals:

$$V_{do} = (2/\pi)\cdot\hat{E} = (2/\pi)\cdot 6\cdot\omega_m\cdot\Psi = 12\cdot f_m\cdot\Delta\Psi_{pp} \quad ; \qquad (31)$$

thus, in order to obtain the maximum value of V_{do} (with the same tooth flux Φ) it is necessary to maximise the flux linkage Ψ.
As regards Ψ, in sinusoidal operation (17) becomes:

$$\overline{\Psi} = \sum_{k_g=1}^{N_t} L_{kg}\cdot\overline{\Phi}_{kg} = \sum_{k_g=1}^{N_t} L_{kg}\cdot\Phi\cdot\exp(j\cdot\theta_{kg}) =$$
$$= \Phi\cdot\sum_{k_g=1}^{N_t} L_{kg}\cdot\exp(j\cdot\theta_{kg}) = M_f\cdot\ell\cdot\Lambda_I\cdot\sum_{k_g=1}^{N_t} L_{kg}\cdot\exp(j\cdot\theta_{kg}) \qquad (32)$$

with θ_{kg} phases of the teeth fluxes Φ_{kg}. Eq. (32) shows that Ψ can be increased both increasing the amplitude Φ of the tooth flux and by summing these fluxes in phase as much as possible; moreover:
- being constant M_f and ℓ, the higher the 1st harmonic Λ_I of the air-gap tooth permeance is, the higher the tooth flux Φ is;
- as regards θ_{kg}, the teeth to be wound are those whose fluxes are almost in phase (or in opposition, if they are wound in the opposite sense); another way (C, D and F) is to subdivide the winding in sub-windings (I and II), exploiting the fact that rectified voltages of series connected bridges (and their average values) can be added without phase problems ($V_{do} = V_{dol} + V_{doII}$).

The amplitude of Λ_I depends mainly on the number of teeth and on the slot dimensions; for a pole shoe with $N_t = 3$ and with the dimensions of Table I, the air-gap tooth permeance (tooth N°1) has the spatial waveform of fig.16.

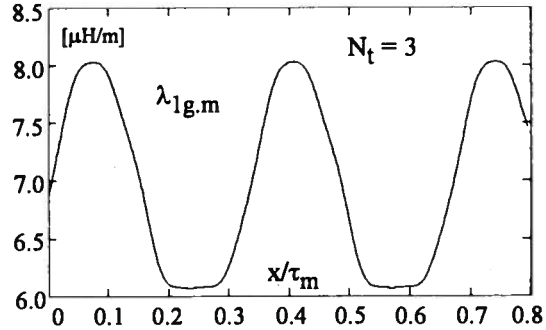

Fig.16 - Permeance at the air-gap of the tooth N°1 of a pole shoe with 3 teeth, with the dimensions of Table I (evaluated by (13)).

The comparison of fig.16 with fig.5 shows a reverse behaviour (here the peaks are at the top), a higher average value (the tooth is more extended) and an apparent equal value of the peak-to-peak fluctuation $\Delta\lambda_{pp}$: actually, from the Fourier series we obtain:

$$\Lambda_{I(Nt=7)} = 0.93\ \mu H/m\ ;\ \Lambda_{I(Nt=3)} = 1.04\ \mu H/m\ ,$$

with a certain prevalence of the case $N_t = 3$ over the case $N_t = 7$.

As regards the phases θ_{kg}, considering that the slot pitch τ_{sg} is the same for all the teeth, also the electrical angle between adjacent teeth (indicated with α_t) is the same, therefore:

$$\alpha_t = \theta_{kg+1} - \theta_{kg} \quad \text{for } kg = 1, \ldots, N_t - 1\ . \qquad (33)$$

Considering that a LSG tooth flux completes a period while this tooth covers the distance τ_{sm}, and that the distance between two adjacent LSG is τ_{sg}, we have (for the symbols, see Table I):

$$\alpha_t/(2\cdot\pi) = \tau_{sg}/\tau_{sm} \quad ; \qquad (34)$$

on the other hand, holding the following equations:

$$\tau_{sg} = (b + b_{sg})/N_t \qquad (35)$$

$$\tau_{sm} = \tau_m/3 \quad , \qquad (36)$$

(34) can be written as:

$$\alpha_t = (6\cdot\pi/N_t)\cdot(b/\tau_m)\cdot(1 + b_{sg}/b) \quad . \qquad (37)$$

The ratios b/τ_m and b_{sg}/b are not constant: thus, (37) shows the non-obvious property that the electrical angle α_t between adjacent teeth of the LSG depends not only on the number of teeth N_t but also (even if weakly) on the geometrical structure of the pole shoe. In practice, if $b/\tau_m \approx 2/3$ and $b_{sg} << b$, we can assume:

$$\alpha_t \approx (4\cdot\pi)/N_t \; . \qquad (38)$$

The insertion of (37) in (32) is of great help in the choice of the winding features, especially when a graphical representation is used: the selection of the teeth to be linked with the winding and of the winding sense (in order to sum the teeth fluxes with the same phase as much as possible) is made easier by diagrams as in fig.17.

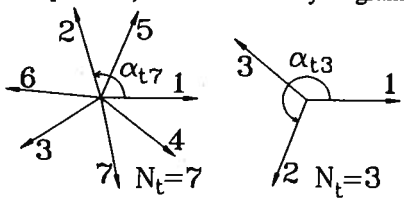

Fig.17 - Phasor diagram of the teeth fluxes: pole shoes with $b/\tau_m = 2/3$, for $N_t = 7$ and $N_t = 3 \Rightarrow \alpha_{t7} \approx 107°$; $\alpha_{t3} \approx 250°$.

Of course, the quantitative characterisation of the winding goodness requires anyway the use of (32) (corresponding to numerically perform the phasor sum of fig.17); to this aim, it is useful to define the number N_ℓ of linked teeth:

$$N_\ell = \sum_{k_g=1}^{N_t} |L_{kg}| \quad . \qquad (39)$$

Eq.(39) indicates which teeth are linked with the winding and how many times, not considering their linking sign.
Thus, we define toothing factor the ratio k_t:

$$k_t = \left| \sum_{k_g=1}^{N_t} L_{kg}\cdot\exp(j\cdot\theta_{kg}) \right| \Big/ N_\ell \quad . \qquad (40)$$

By means of (39) and (40), (32) becomes as follows:

$$\Psi = \Phi\cdot k_t\cdot N_\ell \; . \qquad (41)$$

Eq. (41) is clearly similar to the well known law of phasor sum of the conductor e.m.f.s of a winding; thus, the toothing factor has a close similarity with the winding factor; in fact k_t is a number lower or equal to unity and the product:

$$N_{et} = k_t\cdot N_\ell \qquad (42)$$

can be conveniently defined as effective teeth number: while the toothing factor is a specific parameter, N_{et} represents a global index of the winding goodness.

In the following the V_{do} values are given, in various conditions, evaluated with different methods:

- design method: once the type of winding has been chosen (also by using the diagrams of fig.17), only the presence of M_f and of Λ_I is considered, evaluating V_{do} by means of (31) and (41);
- check method: the complete model of §2 is used, evaluating V_{do} also with the effect of the LSM m.m.f..

As for the calculation of V_{do}, in case of complete model it is possible to remarkably simplify its evaluation: in fact, chosen an instant t_1 (corresponding to the position $x_1(t_1)$) and $t_2 = t_1 + T/6$ (corresponding to the position $x_2 = x_1 + \tau_{sm}$), we have:

$$V_{do} = \frac{6}{T}\cdot\int_{t_1}^{t_2} v_{do}\cdot dt = \frac{6}{T}\cdot\int_{t_1}^{t_2}\left|\frac{d\psi}{dt}\right|\cdot dt = 6\cdot f_m\cdot\int_{x_1}^{x_1+\tau_{sm}}\left|\frac{d\psi}{dx}\right|\cdot dx \; ; (43)$$

Let us choose the position $x_1 = x_m$ in which ψ is minimum; let be x_M the position in which ψ is maximum: if $d\psi/dx$ does not change sign within the intervals x_m-x_M and x_M-x_m (hypothesis always verified in these analyses), from (43) one obtains:

$$V_{do} = 6\cdot f_m\cdot 2\cdot[\psi(x_M) - \psi(x_m)] = 12\cdot f_m\cdot\Delta\psi_{pp} \; . \qquad (44)$$

Thus we have found (31) again: the difference is that here (44) has general validity, with distorted waveform, with $\Delta\psi_{pp} = \psi_M - \psi_m$. Eq.(44) shows that V_{do} depends only on the variation $\Delta\psi_{pp}$ of diagrams like that of fig.12: thus, while the cited irregularities in the permeance contributions (1)-(4) affect the waveform of $e_g(t)$ and of $v_{do}(t)$ (through the derivatives in (18) and in (26), in case they are not filtered by the Fourier series), V_{do} does not depend on them.

Table II shows: V_{dof} (due to the M_f only), for the 6 windings of fig.11, evaluated with the design model (by (31)) and with the harmonic Λ_1 only) (V_{dofp}); V_{dof} evaluated with the check model (by means of (15) and (44), and with the actual waveforms) (V_{dofv}); moreover, the toothing factor is given (k_t), together with the number of linked teeth (N_ℓ), the ratio (winding length)/(active sides length) (ρ_ℓ), the number of bridges (N_b), the number of crossings between end-windings (N_c).

Table II - Comparative analysis of the 6 windings of fig.11 with the field m.m.f. M_f only (N.B.: for subdivided windings and series connected bridges, V_{do} is the sum of the single V_{do}): N_ℓ = number of linked teeth; k_t : toothing factor; N_c : N° of end-winding crossings; V_{dofp} : V_{dof} calculated during the design by (31) and with Λ_I only; V_{dofv} : V_{dof} calculated during the check by (15) and (44); ρ_ℓ : ratio (winding length)/(active side length); n_b : number of bridges.

Winding	V_{dofp} [V]	V_{dofv} [V]	k_t	N_ℓ	ρ_ℓ	N_b	N_c
A	12.37	12.48	0.294	8	1.20	1	2
B	16.70	16.79	0.793	4	1.18	1	2
C	14.90	15.26	0.354	2·4	1.18	2	2
D	20.78	20.94	0.494	2·4	1.21	2	3
E	23.55	22.34	0.982	4	1.33	1	3
F	23.98	22.43	1	2·2	1.25	2	2

The following method remarks can be made:

- the design approach is valid for all cases A, B, C, D ($N_t = 7$);
- the difference between design and check is slightly higher for the cases E, F ($N_t = 3$); the overestimate of V_{do} is due to the most important reducing effect exerted by the 2nd harmonic of the tooth permeance: it reduces the peak-to-peak permeance variation and thus (on the basis of (16) and (44)), the peak-to-peak variation of the flux; this is confirmed in the case F (where the flux linkage coincides with the flux of one tooth): if instead of using the value $\Delta\Lambda_I = 2\cdot\Lambda_I = 2.08$ μH/m, the real peak-to-peak variation of fig.16 is used ($\Delta\Lambda_{pp} = 1.957$ μH/m), $V_{dof} = 22.49$ V is obtained, very close to the check evaluation result.

As regards the results, Table I indicates that:

- being equal the number N_t of pole shoe teeth (thus being equal the tooth flux), the windings with low toothing factor k_t have also low values of the rectified voltage; thus k_t is an effective index of winding goodness;

- for $N_t = 7$, the winding D is that with higher V_{do} (in fact it is the configuration adopted in the prototypes of the Transrapid in Emsland, Germany): on the other hand, it requires two rectifiers, the winding has the highest number of end-winding crossings (3) and the ratio ρ_ℓ (winding length/active side length) is the highest among those for $N_t = 7$;
- again for $N_t = 7$, a valid alternative to the type D is the type B, because the reduction of V_{do} (roughly –20%) is balanced by the use of just one bridge, by the lower number of crossings (2) and by a slightly lower value of ρ_ℓ;
- as regards N_t=3, the value V_{do} of the cases E and F is almost the same: nevertheless, E uses just one bridge, thanks to the fact the tooth flux phasors Φ_1 and Φ_3, almost opposed (see fig.17), are summed in phase ($k_t = 0.982$) by counter-connecting the coils;
- as regards the comparison between the cases $N_t = 3$ and $N_t = 7$, V_{dofE} is higher than V_{dofD}, for two reasons:
  - the amplitude Φ of the tooth flux phasor of the case E is the highest one, mainly because Λ_1 is higher (+12%);
  - in the case E also the toothing factor k_t is higher: this widely balances the fact that the number of teeth linked with the winding E is half of the other; in fact, the number of effective teeth are: $N_{etE} = 3.928$; $N_{etD} = 3.952$;
- as regards the case E, we have also examined the effect of a different LSG slot geometry: if instead of adopting a slot width equal to $b_{sg} = 16$ mm, the same width $b_{sg} = 8$ mm of the pole shoe with 7 teeth is adopted (doubling the slot height, in such a way to contain the same conductor cross-section) we have:
  - being equal the air-gap flux density B_f, the necessary m.m.f. M_f decreases (–4%), thanks to the lower Carter's factor;
  - V_{dof} decreases (–7%), because of the reduction of the toothing factor (–5%) and of the M_f reduction, not compensated by the small increase of Λ_1 (+1%);
  - the slot leakage flux inductance quadruplicates roughly, as like as the voltage drop in the LSG loaded operation;
  - it can be concluded that the wider slot is the best choice.

For the same windings now studied, Table III shows, besides V_{dof}, also the values of V_{do} produced by the LSM m.m.f. only and those with both the m.m.f.s acting at the air-gap.

Table III - Voltage V_{do} of the 6 windings of fig.11 in different operating conditions (check calculations, by (44)):
V_{dof}: V_{do} due to the field m.m.f. only (M_f);
V_{dom}: V_{do} due to the LSM m.m.f. only (m_{mkm});
$V_{dot(\gamma n)}$: V_{do} due to both the m.m.f.s, with $\gamma = \gamma_n$;
$V_{dot(2\gamma n)}$: V_{do} due to both the m.m.f.s, with $\gamma = 2\cdot\gamma_n$

Winding	V_{dof} [V]	V_{dom} [V]	$V_{dot(\gamma n)}$ [V]	$V_{dot(2\gamma n)}$ [V]
A	12.48	5.91	15.16	16.86
B	16.79	5.74	19.26	21.00
C	15.26	5.93	16.52	18.09
D	20.94	8.24	23.88	26.37
E	22.34	4.52	24.64	26.21
F	22.43	8.49	26.05	28.09

As regards the results of Table III, the following can be said:
- V_{dof} due to M_f only is remarkably lower than that produced just by the stator m.m.f.: except for the case E (for which $V_{domE} \approx 0.2\cdot V_{dofE}$), approximately we have: $V_{dom} = (0.3\text{-}0.4)\cdot V_{dof}$;
- V_{dot}, due to the simultaneous effect of the two m.m.f.s, exceeds V_{dof}, produced by the field m.m.f. only, of a quantity roughly constant (approximately +10-20%);
- V_{dot} is weakly dependent on the reaction angle γ, i.e. on the operating conditions of the LSM;
- clearly, the following is verified:

$$V_{dot} \neq V_{dof} + V_{dom} \quad ; \tag{45}$$

the last result is not in contrast with the hypothesis of magnetic linearity, for which the principle of superposition of causes and effects can be applied; in fact, indicated with $\langle\circ\rangle$ the time average value operator, we have (see (28)):

$$V_{dot} = \langle v_{do}(t)\rangle = \langle|e_g(t)|\rangle = \\ = \langle|e_{gf}(t) + e_{gm}(t)|\rangle \neq \langle|e_{gf}(t)|\rangle + \langle|e_{gm}(t)|\rangle = V_{dof} + V_{dom} \tag{46}$$

In conclusion, from the previous remarks we can say that the design model is adequate, also considering the fact that in the LSG loaded operation the rectified voltage V_{dt} decreases compared with V_{dot}, thus becoming roughly equal to V_{dof}.

4. CONCLUSIONS

In the present paper a method for the analysis of design and operation of on-board linear synchronous generators in Maglev vehicles has been described, based on the use of an approximated analytical model of the field at the air-gap: the model, based on the schematization of the flux lines with straight line segments and circumference arcs, allows a simple calculation of the permeance contributions between faced toothed structures, suitably corrected with the Carter's factor: the comparison with the results obtained by the Finite Element Method is satisfying.

The relationships for the evaluation of the teeth fluxes at the air-gap have been developed, in particular for the contributions due to the m.m.f. produced by the alternative currents of the LSM.

Waveforms have been obtained for the tooth flux, the winding flux linkage, the induced e.m.f.s and the no-load rectified voltages.

A design method, valid for evaluating the rectified voltage generated by the field m.m.f. only (prevailing compared with the other contributions), has been developed: it uses only the first harmonic of the Fourier series of the tooth permeance at the air-gap, and it leads to phasor diagrams useful to guide the design.

The average values of the LSG rectified voltage, for a number of winding kinds and operating conditions have been evaluated, thus comparing their functional and constructional features.

The research will continue, according to different goals:
- extension of the analysis to the LSG loaded operation;
- analysis of new configurations of LSG windings, for their performance optimisation;
- analysis of operation in case of unbalanced and distorted stator currents (inverter supply).

REFERENCES

[1] A. Di Gerlando, I. Vistoli, M. Galasso: "Comparative Analysis of EDS and EMS Maglev Systems", Maglev'93, 13th International Conference on Magnetically Levitated Systems and Linear Drives, Argonne National Laboratory, Illinois, USA, May 1993, pp.336-341

[2] A. Di Gerlando, I. Vistoli: "Design Problems of Linear On Board Generators in EMS Maglev Transportation Systems", Ibidem, pp.342-347

[3] A. Di Gerlando, I.. Vistoli: "Analisi di progetto di generatori lineari di bordo per veicoli Maglev di tipo EMS"; Atti del 1° Convegno Nazionale Progetto Finalizzato Trasporti 2 del CNR, Roma Italia, 1993 (in Italian), pp.1489-1508.

[4] C. C. Hawkins: "The Dynamo", I. Pitman and Sons Ltd. Pub., 1922, Vol.1, p.494.